

Facile sonochemical preparation of size controlled bismuth hydroxide and oxide nanostructures in the presence of polyvinyl alcohol (PVA) as a capping agent

FARZAD SEDAGHATDOUST-BODAGH^a, YASHAR AZIZIAN-KALANDARAGH^{a,b*}

^aDepartment of Physics, University of Mohaghegh Ardabili, Ardabil, Iran

^bDepartment of Engineering Sciences, Sabalan University of Advanced Technologies (SUAT), Namin, Iran

A simple ultrasound-assisted method involving polyvinyl alcohol (PVA) was employed to prepare the size controlled bismuth oxide and bismuth hydroxide nanostructures. The XRD study confirms the structure of the system as cubic with β - Bi_2O_3 phase. Scanning electron microscopy revealed that the β - Bi_2O_3 and bismuth hydroxide samples composed of cube like structures. The SEM micrographs also show the improvement in the particle size distribution upon PVA capping agent addition. Absorption spectra have been obtained using a UV-Vis spectrophotometer to find the optical direct band gap. The optical gap of pure and PVA capped bismuth oxide and bismuth hydroxide nanomaterials have been calculated using the Tauc's relationship and blue shift in the optical gap has been reported. We also found that the optical band gap (E_g) increases with the increase in molar concentration of the PVA. Fourier transform infrared (FT-IR) spectra of the prepared samples show the presence of characteristic bands for the PVA in the spectrum and reveal the capping effect of PVA on bismuth oxide and hydroxide nanostructures.

(Received February 3, 2017; accepted October 10, 2017)

Keywords: Crystal structure, Optical properties, Electron microscopy (SEM), Fourier transform infrared spectroscopy (FT-IR), Nanostructures

1. Introduction

The interest for the preparation and application of nanometer size materials is increasing since they exhibit better properties for industrial and technological applications [1-3]. Size-controlled preparation of oxide semiconducting nanostructures is a great challenge in materials science because their intrinsic chemical and physical properties are strongly dependent on the size-induced quantum confinement effects. There has been a great deal of interest in developing physiochemical methods for controlling the nanostructures sizes and shapes using organic capping agents [4-7]. Various organic capping materials, with different head groups, hydrophobic chains, counterions, and molecular architectures, have been widely employed as capping or inducing agents to control the nucleation, growth and assembly of metal oxide nanostructures. Particularly, PVA is a most frequently used for the synthesis of metal oxide nanostructures in aqueous solution [8-10]. Between different metal oxide materials bismuth oxide is an important semiconductor material which has been used widely in the fields of medicine [11] catalysis [12], functional ceramics [13], superconductor materials [14] energy materials [15], and optical materials [16], owing to its special properties of wide band gap, high refractive index, photoluminescence and photoconductivity. There are six polymorphs of bismuth oxide named α - Bi_2O_3 , β - Bi_2O_3 , γ - Bi_2O_3 , δ - Bi_2O_3 , ω - Bi_2O_3 and ϵ - Bi_2O_3 . The bismuth oxide polymorphs have significantly different electrical and optical properties [17,

18]. It was reported that β - Bi_2O_3 is a p-type semiconductor with a band gap of about 2.5eV [19]. Many methods such as high-temperature oxidation of bismuth metal [20], pyrolysis of bismuth compound [21], one step aqueous method [22], chemical vapor deposition (CVD) [23], simple two-step solution phase approach [24] sol-gel process [25], magnetron sputtering deposition [26], crystallization in glass matrix [27], template-based heat treatment [28], thermal evaporation [29], room temperature chemical solution route [30], metalorganochemical vapor deposition [31], surfactant-assisted hydrothermal synthesis [32], and ultrasound-assisted method [33], have been developed for preparation of bismuth oxide nanomaterials. Nano and microstructures with anisotropic shapes and morphologies and high surface to volume ratio are aseptically attractive due to their higher photocatalytic activity [34, 35]. Among them, ultrasound-assisted method is very simple and has evident advantages due to good compositional control, low equipment cost and lower crystallization temperature. In the present work, we report the ultrasound-assisted method for preparation of β - Bi_2O_3 nanostructures. The ultrasound-assisted methods involve ultrasound irradiation of the precursor during synthesis. Ultrasound irradiation has been used extensively to produce novel materials with interesting properties. Because of the immense physical and chemical effects of ultrasonic waves in solutions, by using this method we can produce materials with novel properties. The particle size and morphology of bismuth oxide and bismuth hydroxide nanostructures give rise the most important changes in the properties of nanomaterials.

The controlled preparation of nanostructures with different sizes and morphologies is a challenging research area [36-39].

In summary, bismuth oxide and bismuth hydroxide nanostructures were prepared by ultrasound-assisted method in the presence of PVA as a capping agent. In addition, the particle size was tuned by variation of the concentration of capping agent. The morphology and size of bismuth oxide and bismuth hydroxide nanostructures were analyzed by means of scanning electron microscopy (SEM). The band gap of the Bi_2O_3 nanocrystals was calculated by the obtained results from UV-Visible spectroscopy. Fourier transform infrared spectroscopy (FT-IR) and X-ray diffraction (XRD) were used to characterize all of the prepared samples, showing that nanosized bismuth oxide and bismuth hydroxide particles were dispersed uniformly.

2. Materials and methods

2.1. Preparation of bismuth hydroxide and $\beta\text{-Bi}_2\text{O}_3$ nanostructures

All of the reactants and solvents were analytical grade and were used without any further purification. The experimental procedures are as follows: Aqueous solution of bismuth nitrate (0.2M) was prepared by dissolving of 1.94g of the salt in 20mL of double distilled water at $\text{pH} = 1$. This solution was irradiated with a high intensity ultrasonic at room temperature for 15min using Dr. Heilscher ultrasound processor (UP200H Germany, 14mm diameter Ti horn, 200W/cm², 24 kHz). Different amounts of aqueous solution of PVA (3% and 5%) were added to the solution and the effects of addition were characterized. During the sonication of the reaction mixture, the temperature was increased to 80°C as measured by mercury thermometer. The prepared suspension was centrifuged to get the precipitate out and washed three times using double distilled water and ethanol to remove the unreacted reagents and dried in an oven at 60°C for 24h. To convert the as-prepared $\text{Bi}(\text{OH})_3$ nanostructures to

$\beta\text{-Bi}_2\text{O}_3$, the as-prepared powders were annealed at 300°C for 1h in open air.

2.2. Instruments

The X-ray diffraction (XRD) patterns of products were recorded on a Philips X'pert X-ray diffractometer with Cu K α radiation ($\lambda=1.54056 \text{ \AA}$) employing a scanning step of 0.02°S^{-1} , in 2θ range from 20° to 80° . Surface morphologies were studied using the LEO1430 VP scanning electron microscope (SEM) with 15kV accelerating voltages. UV-Vis absorption spectra of the samples were obtained using a Shimadzu spectrophotometer (Japan, model 1650). Fourier transform-infrared (FT-IR) spectra were obtained using Perkin Elmer Spectrum RXI apparatus. Thermal analyses were done using a thermogravimetric apparatus (model: Linseis, STA PT-1000).

3. Results and discussion

3.1. X-ray diffraction

The structural properties of PVA-capped bismuth hydroxide and $\beta\text{-Bi}_2\text{O}_3$ nanostructures were studied by X-ray diffraction method. Figures 1(A, B and C) and 2(A, B and C) show the XRD patterns of prepared samples at different capped agent concentration (A without capped agent, B contain 3% PVA concentration and C contain 5% PVA). In the case of figure 1(A, B and C), different kinds of bismuth oxide and bismuth hydroxide were formed. The formation of different phases of bismuth oxide and hydroxides depends directly on the synthesis temperature. In Fig. 2, all diffraction peaks can be readily indexed to the cubic $\beta\text{-Bi}_2\text{O}_3$ nanoparticles (PDF card No. 78-1793, space group $P\bar{4}2_1c$ (114), unit cell parameters $a=7.741(3)$, $c=5.634(2) \text{ \AA}$ at RT, $Z=4$; also card No. 27-0050) [40]. No other peaks were observed such a Bi or any other Bi based oxides, which shows purity of the bismuth oxide samples. The diffraction peaks are broadened with increasing in the capping agent concentration, which indicates that the crystalline sizes of samples are small.

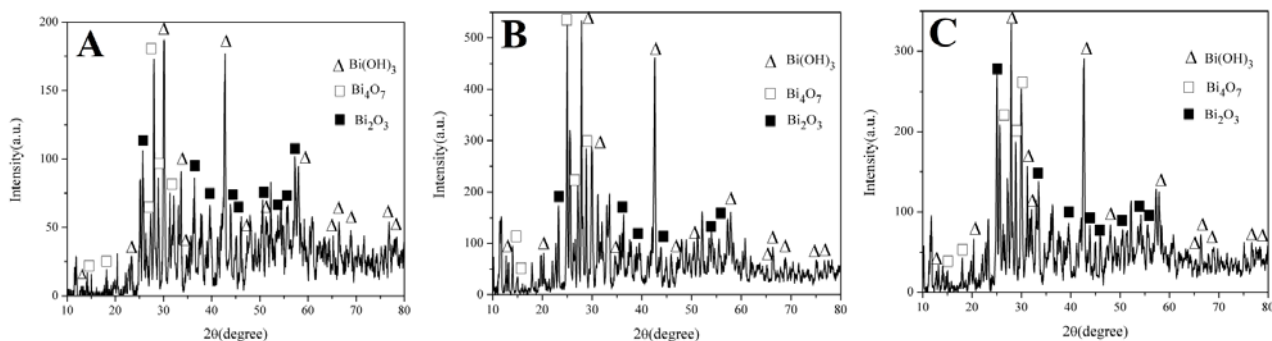


Fig. 1. X-ray diffraction patterns of bismuth hydroxide samples at different capping agent concentration: (A) without capping agent, (B) containing 3% PVA and (C) containing 5% PVA

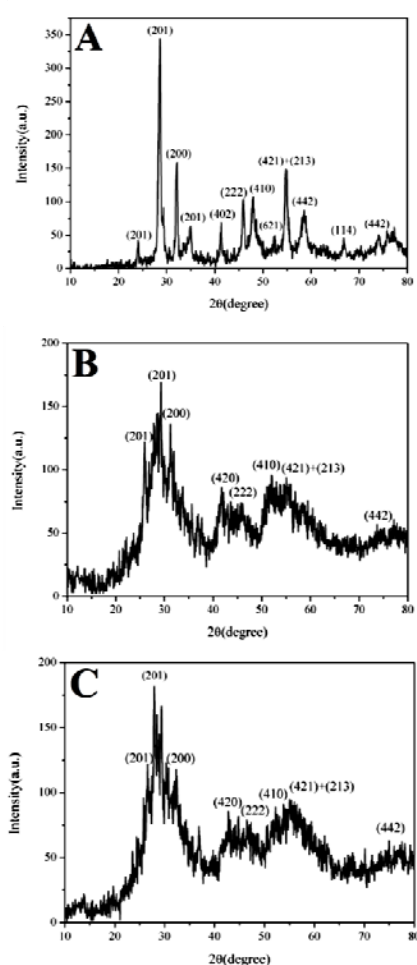


Fig. 2. X-ray diffraction patterns of bismuth oxide samples at different capping agent concentration, (A) without capping agent, (B) containing 3% PVA and (C) containing 5% PVA

The mean crystallite size of bismuth hydroxide and β - Bi_2O_3 nanostructures was calculated using Debye-Scherrer's equation:

$$D = 0.94 \lambda / \beta \cos \theta \quad (1)$$

Where D is the mean crystallite size, λ is the X-ray wavelength, β is the full-width at half maxima of the prominent peak and θ is the diffraction angle corresponding to the peak [41]. For bismuth hydroxide samples we only consider bismuth hydroxide peaks and the crystallite sizes was calculated to be 24, 18 and 17nm for samples prepared with 0%, 3% and 5% PVA concentration, respectively. In the case of β - Bi_2O_3 the corresponding nanoparticles sizes were calculated to be 23, 18 and 15nm. The measured sizes reveal clearly that with increasing PVA concentration the crystallite size decreases gradually.

3.2. TGA

The crystalline phase transitions of the as-prepared sample have been characterized by TGA analysis. In Fig. 3, the restructuring of the prepared nanostructures occurs at different temperatures. We believe that the observed

fluctuations at different temperature probably related to the releasing of water molecules from the outer shells of the prepared nanopowders and also maybe the crystalline phase transitions of different structures formed in unannealed samples. The existence of different crystalline phase in unannealed sample was observed in XRD patterns and transition to pure β - Bi_2O_3 nanostructures also confirmed by XRD patterns.

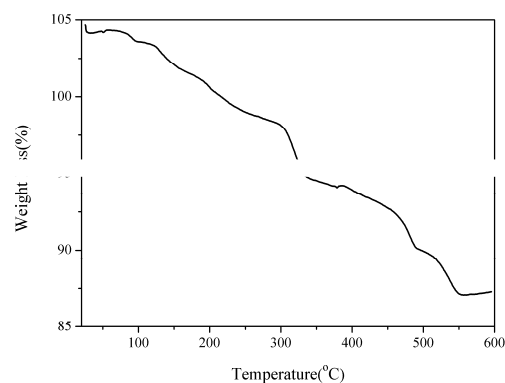


Fig. 3. TGA analyses of bismuth hydroxide

3.3. UV-Vis spectroscopy

The optical properties of the prepared samples were studied in the wavelength region of 100-800nm and the optical band gap is calculated for the nanostructures. Figs. 4(a) and 5(a) show the optical absorbance edge of the as-prepared samples A, B and C for bismuth hydroxide and oxide, respectively. The absorbance edges of samples revealed clearly that with increasing PVA concentration, the absorbance wavelengths were shortened. The samples show strong absorption below 400nm and blue shift of the absorption edge compared to that for the bulk bismuth hydroxide and bismuth oxide (typically takes place at 496nm) [18]. When the quantum confinement effect occurs the blue shift in energy is observed. The band gap energy is particle size dependent and increases with decreasing particle size.

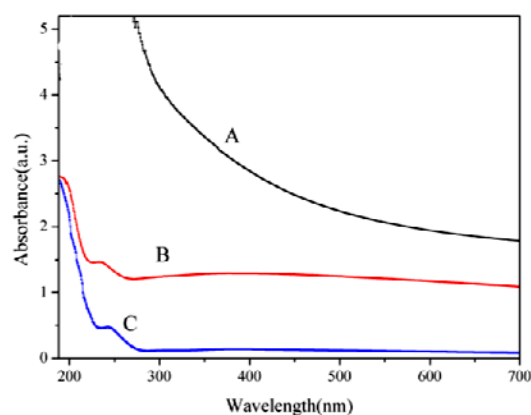


Fig. 4(a). UV-Vis spectra of bismuth hydroxide samples at different capping agent concentrations, (A) without capping agent, (B) containing 3% PVA and (C) containing 5% PVA

For crystalline semiconductor, the optical absorption near the band edge follows the equation

$$\alpha h\nu = A(h\nu - E_g)^{n/2} \quad (2)$$

Where α , ν , E_g and A are the absorption coefficient, the light frequency, the band gap and a constant, respectively [42]. Figs. 4(b) and 5(b) show the Tauc plot of the as-prepared samples A, B and C for bismuth hydroxide and oxide, respectively.

The corresponding band gap energy for the bismuth hydroxide samples was calculated 2.94, 4.15 and 4.28eV.

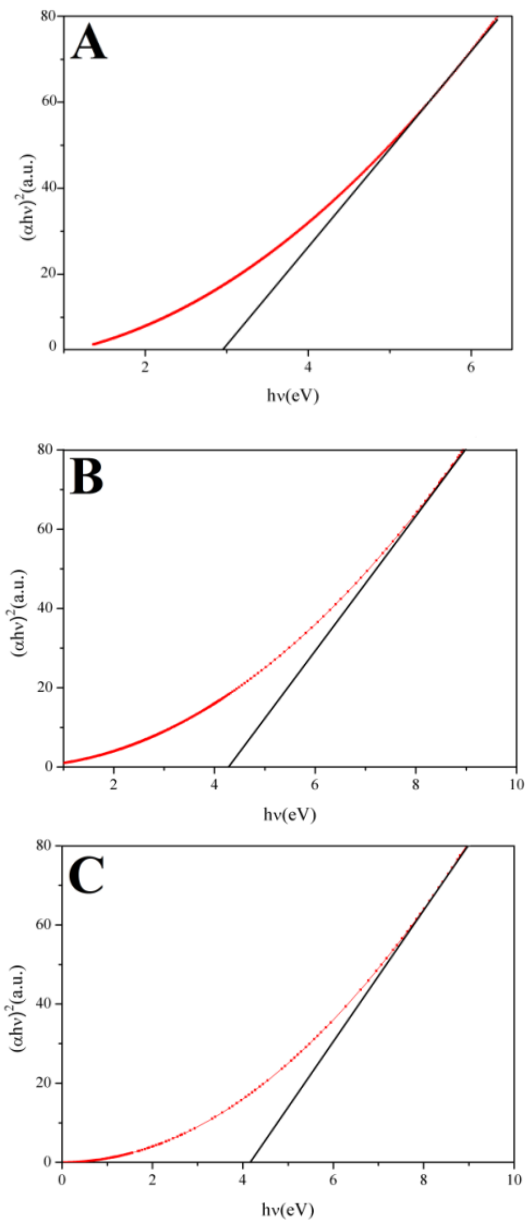


Fig. 4(b). Tauc plot of bismuth hydroxide samples, (A) without capping agent, (B) containing 3% PVA and (C) containing 5% PVA

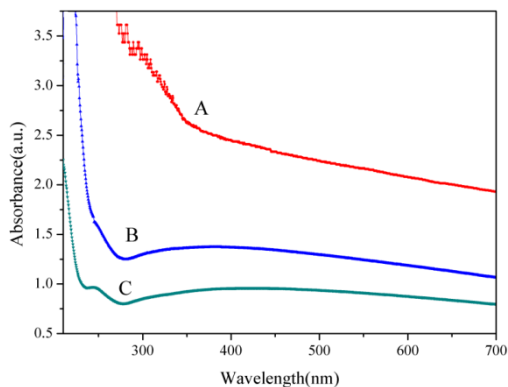


Fig. 5(a). UV- Vis spectra of bismuth oxide samples at different capping agent concentration, (A) without capping agent, (B) containing 3% PVA and (C) containing 5% PVA

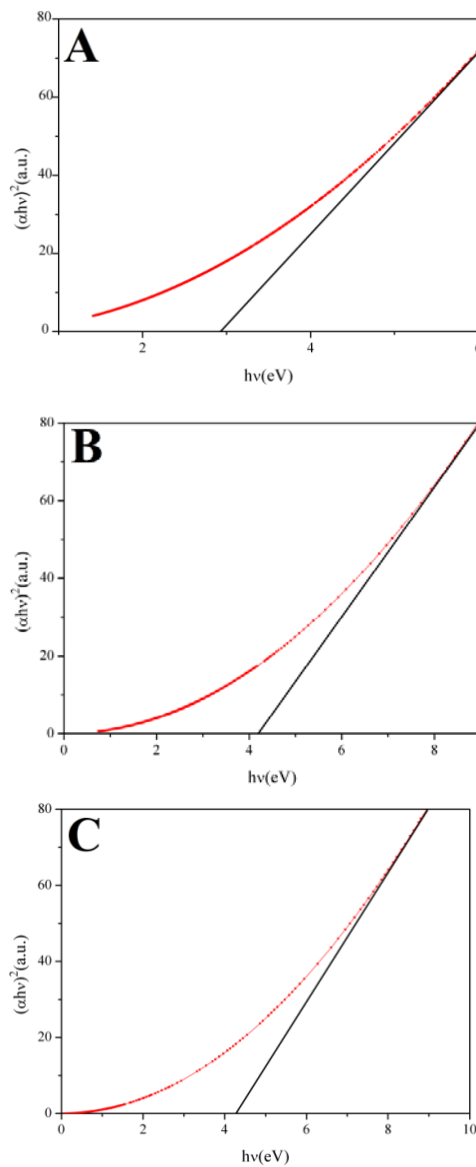


Fig. 5(b). Tauc plot of bismuth oxide samples, (A) without capping agent, (B) containing 3% PVA and (C) containing 5% PVA

The corresponding band gap energy for bismuth oxide samples was calculated 2.93, 4.19 and 4.30eV. The increasing of the band gap energy is due to decreasing particle size of samples.

3.4. SEM

Figs. 6 and 7 show the scanning electron microscopy analysis (SEM) for the powders synthesized under ultrasound wave with different amount of PVA capping agent. Images show the influence of the capping agent contents on the bismuth hydroxide and bismuth oxide. Adding capping agent affect the morphology and sizes of the prepared nanostructures.

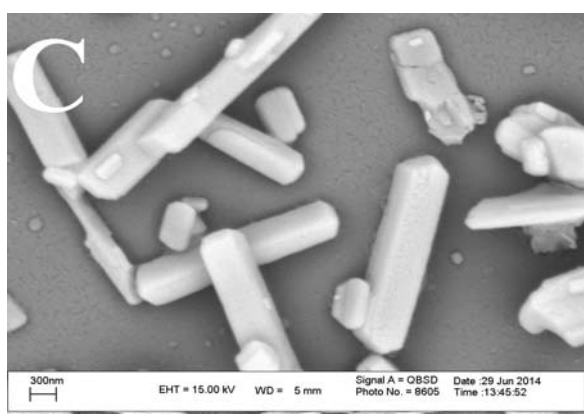
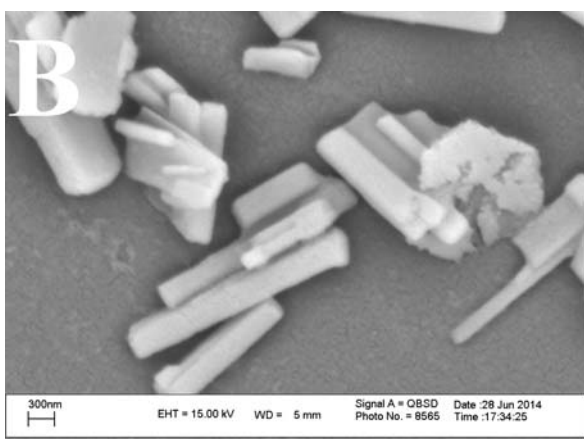
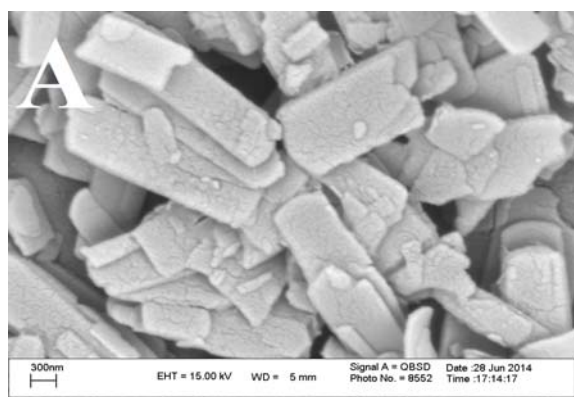


Fig. 6. SEM images of bismuth hydroxide samples, (A) without capping agent, (B) containing 3% PVA and (C) containing 5% PVA

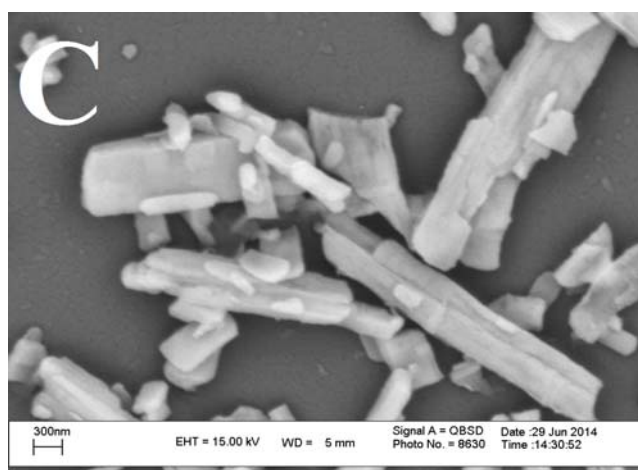
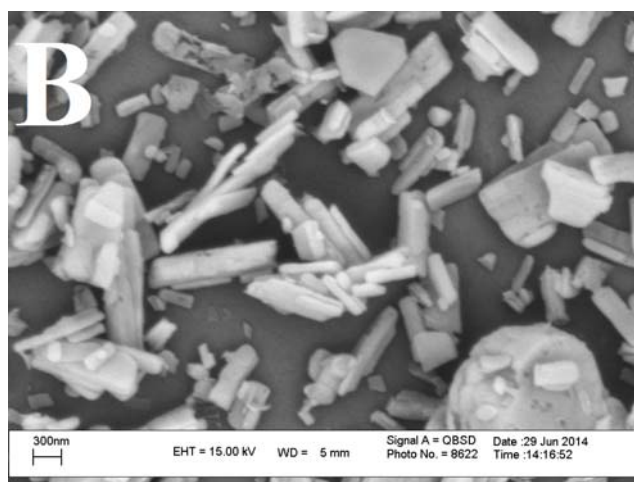
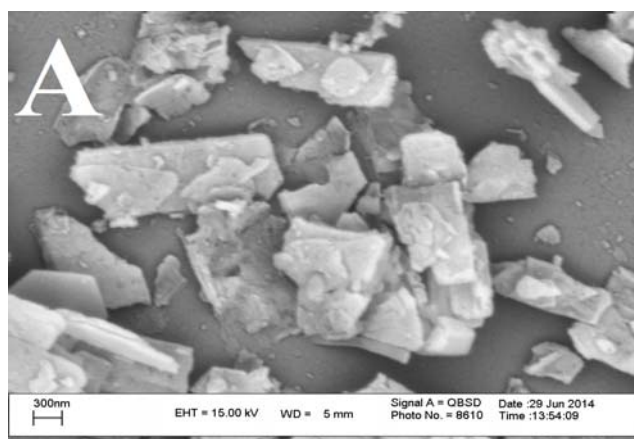


Fig. 7. SEM images of bismuth oxide samples, (A) without capping agent, (B) containing 3% PVA and (C) containing 5% PVA

There is a difference between the uncapped sample and PVA-capped samples: In as uncapped sample the particles formed in the sheet-like shape which aggregated in the form of polydisperse micron sized aggregated, but in the PVA-capped samples, nanostructures formed in a rod-like shape, with increasing the percent of capping agent the average of diameter of rods decreased. However, a polydispersity nature is observed in all prepared samples.

3.5. FT-IR

In the order to study the underlying adsorption mechanism of PVA onto the nanoparticle surface, FT-IR analysis of PVA-capped bismuth hydroxide and bismuth oxide was carried out and the obtained data were compared with uncapped sample. Figs. 8 and 9 show the FT-IR spectra of bismuth hydroxide and bismuth oxide respectively.

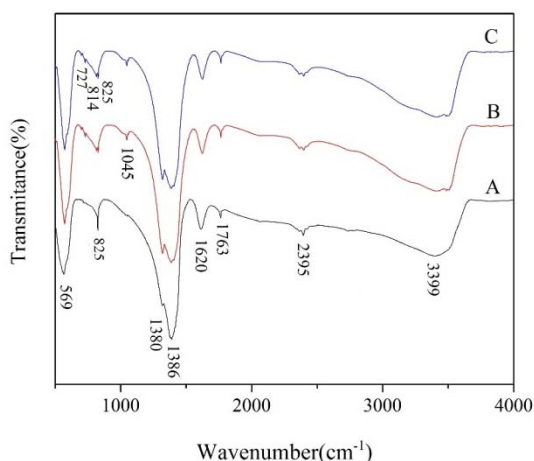


Fig. 8. FT-IR spectra of bismuth hydroxide samples at different capping agent concentration, (A) without capping agent, (B) containing 3% PVA and (C) containing 5% PVA

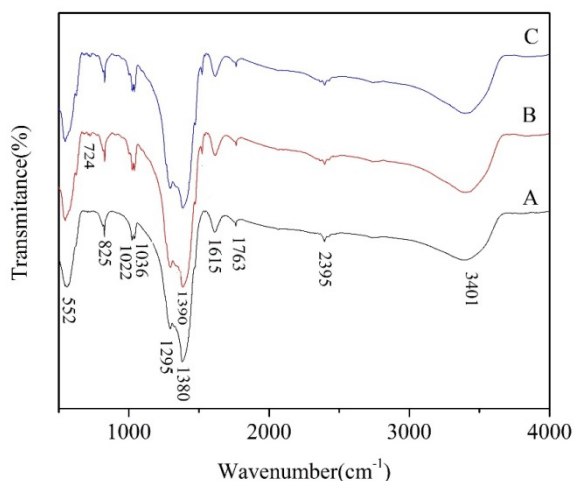


Fig. 9. FT-IR spectra of bismuth oxide samples at different capping agent concentration, (A) without capping agent, (B) containing 3% PVA and (C) containing 5% PVA

The broad absorption band around 3400cm⁻¹ corresponds to the O-H stretching vibration of adsorbed water molecules on the samples [43]. The peak at 2395cm⁻¹ is related to BiO-H stretching vibration in the as-prepared sample which completely disappeared after the annealing process [44]. The peaks at 810 to 1045cm⁻¹ are also corresponded to the stretching of bismuth oxide material [45]. The peak around 720cm⁻¹ is attributed to

stretching vibration in C-O. In the case of bismuth hydroxide nanocrystals also the same results obtained, but another peak around in 1045cm⁻¹ appears which is due to the C-H bending vibration [46]. A comparative analyses shows, with addition of PVA as a capping agent to bismuth oxide and hydroxide materials the energy between functional groups in changed and some peaks show a slight shift which confirms the formation of composition of PVA and bismuth oxide and hydroxides.

4. Conclusion

We have prepared bismuth oxide nanostructures with different concentration of PVA and their optical and morphological properties were investigated by different analysis. Quantum size effect observed from the optical absorption spectra, which showed blue shift in compared to the bulk bismuth oxide. The analyses of SEM, XRD and absorption edge of the prepared samples showed that the amount of capping agent affect the structural and optical properties of nanostructures. Broadness in XRD peaks, blue shift in UV-Vis peak and appearance of some peaks in FT-IR spectrum confirm the formation of very fine nanostructures and the size of these nanostructures can be controlled by the amount of capping agent material. The morphological analysis using SEM images also confirms the formation of rod-like nanostructures by increasing of capping agent amounts. Also the images show more monodispersity in high density of capping agent.

References

- [1] F. Bayrakceken Nisancl, U. Demir, American Chemical Society **28**, 8571 (2012).
- [2] F. Zhou, Q. Liu, J. Gu, W. Zhang, D. Zhang, Journal of Power Sources **273**, 945 (2015).
- [3] C. Nabais, R. Schneider, C. Bellouard, J. Lambert, P. Winmann, D. Billaud, Material Chemistry and Physics **117** 268 (2009).
- [4] G. Anandha Babu, G. Rari, Y. Hayakawa, M. Kumaresavanji, Journal of Magnetic Materials **375**, 184 (2015).
- [5] S. Soleimani, A. Salabat, R. F. Tabir, Journal of Colloid and Interface Science **426**, 287 (2014).
- [6] B. Ajita, Y. Ashok Kumar Reddy, P. Sreedhara Reddy, Powder Technology **269**, 110 (2015).
- [7] L. Wang, X.T. Tao, J.X. Yang, Y. Ren, Z. Liu, M. H. Jiang, Opt. Mater. **28**, 1080 (2006).
- [8] H. Zhaou, L. Zheng, H. Jia, Colloid and Surfaces A: Physicochemical and Engineering Aspects **45**, 9 (2014).
- [9] G. W. Hepburn, Batchelor-Mc Auley, C. Tschulik, K. Torabi Kachoosangi, R. Ness. D. Campton. Sensors and Actuators B: Chemical **204**, 445 (2014).
- [10] G. Ghosh, M. Kanti Naskar, A. Patra, M. Chatterjee, Opt. Mater. **28**, 1047 (2006).

- [11] Y. Nan, S. Hong-Zhe, *Coord. Chem. Rev.* **25**, 2354 (2007).
- [12] J. Sheng-Ming, T. Mo-Tang, Y. Wei-Jun, *J. Cent. South Univ. Tech.: Nat. Sci.* **32**, 247 (2001).
- [13] Z. Lazerevic, B. D. Stonavic, J. A. Varela, *J. Sci. of Sint.* **37**, 199 (2005).
- [14] M. V. Makarov, P. E. Kazin, Y. D. Teryakov, M. Jansen, M. Reissner, W. Steiner, *Phys. C.* **419**, 61 (2005).
- [15] J. Zhi-Yi, Z. Lei, C. Li-li, X. Chang-Rong, *J. Electrochemical. Acta.* **54**, 3059 (2009).
- [16] M. Mehring, *Coord. Chem. Rev.* **251**, 974 (2007).
- [17] K. S. Martirosyan, L. Wang, A. Vicent, D. Luss, *Nanotech.* **20**, 405 (2009).
- [18] Y. Qiu, M. Yang, H. Fan, Y. Zuo, Y. Shao, Y. Xu, X. Yang, S. Yang, *Cryt Eng Comm.* **13**, 1843 (2010).
- [19] X. Xiao, R. Hu, C. Lio, C. Xing, C. Qian, X. Zuo, J. Nan, L. Wang, *App. Catal. B: Env.* **140-141**, 433 (2013).
- [20] K.S. Martirosyan, L. Wang, A. Vicent, D. Luss, *Nanotech.* **20**, 405 (2009).
- [21] L. Madier, S. E. Pratsinis, *J. Amer. Cer. Soc.* **85**, 1713 (2002).
- [22] W. Yi, Z. Jingzhe, W. Zichen. *Coll. Surf. A; Physicochem. Eng. Asp.* **377**, 409 (2011).
- [23] H. Jung, C. F. Feldmann, *J. Mat Sci.* **36**, 297 (2001).
- [24] P. Arun-Prakash, Y. Singying, C. Shen-Ming, *Talanta* **87**, 15 (2011).
- [25] W. He, W. Qin, X. Wu, X. Ding, L. Chen, Z. Jiang, *Thin Solid Films* **515**, 5362 (2007).
- [26] B. Sirota, J. Reyes-Cuellar, P. Kohli, L. Wang, M. E. McCarroll, S. M. Aouadi, *Thin Solid Films* **520**, 6118 (2012).
- [27] S.M. Abo-Naf, R.L. Elwan, G.M. Elkomy, *J. Non-Cryst. Sol.* **358**, 964 (2012).
- [28] B. J. Yang, M. S. Mo, H. M. Hu, C. Li, X. G. Yang, Q. W. Li, Y. T. Qian, *Eur. J. Inorg. Chem.* **9**, 1785 (2004).
- [29] X. P. Shen, S. K. Wu, H. Zhao, Q. Liu, *Phys. E.* **39**, 133 (2007).
- [30] X. Gou, R. Li, G. Wang, Z. Chen, D. Wexler, *Nanotech.* **20**, 495501 (2009).
- [31] H. W. Kim, J. H. Myung, S. H. Shim, C. Lee, *Appl. Phys. A: Mater. Sci. Process.* **84**, 187 (2006).
- [32] H. Lu, S. Wang, L. Zhao, B. Dong, Z. Xu, J. Li, *RSC Adv.* **2**(8), 3374 (2012).
- [33] Y. Azizian-Kalendaragh, F. Sedaghatdoust-Bodagh, A. Habibi-Yangjeh, *Superlattices and Microstructures* **81**, 51 (2015).
- [34] P. D. Dimple, M. Roy, A. K. Tyagi, *Dalton Trans.* **41**, 10238 (2012).
- [35] S. Eftekhari, A. Habibi-Yangjeh, S. Sohrabnezhad, *J. Hazard. Mat.* **178**, 349 (2010).
- [36] Y. A. Kalendaragh, M. B. Muradov, R. K. Mamedov, M. Behboudnia, A. Khodayari, *Optoelectron. Adv. Mat.* **2**, 42 (2008).
- [37] Y. Azizian-Kalendaragh, *Optoelectron. Adv. Mat.* **4**, 174 (2010).
- [38] Y. Azizian-Kalendaragh, S. Özçelik, *Optoelectron. Adv. Mat* **10**, 537 (2016).
- [39] R. Shokrani-Havigh, Y. Azizian-Kalendaragh, *J. Optoelectron. Adv. M.* **19**, 283 (2017).
- [40] PDF cards No.: 78-1793; 27-50050; 71-0465; 41-1449; 82-1491, International Centre for Diffraction Data, Joint Committee on Powder Diffraction Standards, Powder Diffraction File, 1601 Park Lane, Swarthmore, PA 19081, USA.
- [41] N. Dipesh, *Journal of Science* **8**, 83 (2012).
- [42] J. Barman, K. C. Sarma, M. Sarma, K. Sarma, *Indian Journal of Pure and Applied Physics* **5**, 339 (2008).
- [43] M. Bosca, L. Pop, G. Borodi, P. Pascuta, M. Culea, *Alloys Compd.* **479**, 579 (2009).
- [44] F. He, J. Wang, D. W. Deng, *Alloys Compd.* **509**, 6332 (2011).
- [45] M. Ristic, S. Popovic, S. Music, *Mater. Letters.* **58**, 2494 (2004).
- [46] H. Zhu, Y. Li, R. Qiu, L. Shi, W. Wu, S. Zhou, *Biomaterials* **33**, 3058 (2012).

*Corresponding author: yashar.a.k@gmail.com,
azizian@uma.ac.ir